Biochemical and Biophysical Research Communications 616 (2022) 122–128

Contents lists available at ScienceDirect

Biochemical and Biophysical Research Communications

journal homepage: www.elsevier.com/locate/ybbrc

Structural insights into the binding of nanobody Rh57 to active RhoA-GTP

Yiran Zhang, Shihao Cheng, Peiyu Zhong, Ziying Wang, Rui Liu**, Yu Ding*

State Key Laboratory of Genetic Engineering, School of Life Sciences, Fudan University, Shanghai, 200438, China

ARTICLE INFO

Article history:
Received 14 May 2022
Accepted 27 May 2022
Available online 29 May 2022

Keywords:
RhoA
Nanobody
Rh57
GTP
Structure
Epitope

ABSTRACT

RhoA protein is a small GTPase that acts as a molecular switch. When bound to guanosine triphosphate (GTP), RhoA can activate several key signal pathways. Recently, nanobody Rh57 specific binding with GTP bound active RhoA was discovered and developed as a BRET biosensor without cytotoxicity. To further clarify the nanobody Rh57's mechanism of action, we co-expressed, purified, and crystallized the RhoA-Rh57 nanobody complex and solved the structure by X-ray diffraction with a resolution of 2.76 Å. The structure showed that the interaction is mainly through hydrogen bonds, salt bridges, aromatic-aromatic interactions, and hydrophobic interactions. The involved regions include CDR3 and non-hypervariable loop of Rh57, and the SWI switch loops of RhoA, respectively. The different SWI conformation of inactivated RhoA-GDP prevented the Rh57's binding. The possible explanation of Rh57 as a non-cytotoxic BRET intracellular tracer is that Rh57's binding did not overlap with downstream PRK1 and thus did not interfere with the downstream signaling pathway. Our research provides an in-depth understanding of how nanobodies recognize activated RhoA-GTP while not binding inactivated RhoA-GDP. This structural information may also provide critical information for further optimization of relevant nanobodies.

1. Introduction

Rho GTPases are Ras homologous (Rho) proteins that act as molecular switches [1]. When bound to guanosine triphosphate (GTP), Rho GTPases can activate key signal pathways that regulate many cellular responses, such as actin cytoskeleton dynamics, cell cycle, cell migration, and cell adhesion [2,3]. The signal pathways are switched off when Rho GTPases are bound to Guanosine diphosphate (GDP). While Rho GTPases transit to a GTP-bound active state, they trigger downstream signaling pathway effectors [2]. Rho family contains more than 20 members, including RhoA, Rac1, and Cdc42 [1]. Previous studies have shown that multiple pathogenic mutations in critical members of the Rho subfamily, such as RhoA, can lead to malignant tumor proliferation and metastasis. Therefore, this subfamily has become an essential target in anti-tumor drug research and development. Many previous studies related to RhoA have shown that RhoA promotes the formation of actin stress fibers and the assembly of focal adhesion [4]. Its overexpression or activation may lead to the migration or metastasis of cancer cells [5]. When the activity of the RhoA protein is uncontrolled upregulated, it can destroy the epithelial surface tissue, increase cell movement and promote the degradation of the extracellular matrix to promote the metastasis of tumor cells [6]. Other evidence indicates that RhoA protein may protect cells from apoptosis [5].

When the GDP-binding RhoA shifts to the GTP-binding state, the signal effector can specifically recognize the subtle conformation change [7]. Currently, several RhoA inhibitors have been intensively investigated, such as the small molecule inhibitor Rhosin, which inhibits the interaction of Rho with several guanine nucleotide exchange factors (GEFs). However, the efficiency of this inhibitor is limited in cellular assays [8,9]. One of the difficulties in developing effective and efficient RhoA inhibitors is the lack of quantitative tools that can accurately monitor the level of GTP binding active RhoA in living cells. Therefore, biosensors that can detect the activated RhoA with high selectivity and stability are urgently needed.

Nanobodies (Nbs) are a kind of smallest biomolecules with

Abbreviations: GTP, guanosine triphosphate; GDP, guanosine diphosphate; GMP-PNP, Guanylyl imidodiphosphate; Nb, nanobody; CDR, Complementarity determining region; DLS, dynamic light scattering; BRET, bioluminescence resonance energy transfer.

* Corresponding author.
** Corresponding author.
E-mail addresses: liur@fudan.edu.cn (R. Liu), yuding@fudan.edu.cn (Y. Ding).

https://doi.org/10.1016/j.bbrc.2022.05.084
0006-291X/

excellent binding affinity to the target protein than small molecular weight compounds. Casterman et al. first discovered a type of functional antibodies lacking light chains in camels in 1993 [10]. Researchers later reconstituted these antibodies into particular, biologically active antibodies called nanobodies due to their small molecular weight (12–15 kDa) [11]. Unlike traditional antibodies, nanobodies have significant advantages in size, exhibit ultra-high stability and solubility, and show less steric hindrance after binding to antigen [12]. Nanobodies are widely used in fields such as the industry in vitro diagnostics (IVD) [13] and clinical applications [14]. Previously, Olichon and colleagues screened out two kinds of nanobodies named Rh12 and Rh57 binding to RhoA [9,15]. Although Rh12 has high specificity and affinity for the GTP-binding form of RhoA in vitro and in cells, it significantly affects cell shape associated with actin polymerization defects [15]. It is unsuitable for developing into an active form RhoA biosensor. Rh57 also has high specificity and affinity for the GTP-binding form of RhoA and does not affect the intracellular RhoA function, and is further developed as a RhoA biosensor molecule in BRET assay [9].

However, no structure of GTP binding activated RhoA with nanobody is solved. Rh57 nanobody can selectively bind to activated GTP binding RhoA but does not interact with GDP binding RhoA. The mechanism of Rh57's binding while not affecting RhoA's downstream intracellular function is also unknown. Therefore, we intend to determine the crystal structure of the RhoA-Rh57 complex and gain insight into its binding mechanism. In this study, we simultaneously expressed RhoA and its nanobodies, purified the protein complex, determined the complex structure of RhoA-Rh57 by X-ray diffraction, and obtained atomic-scale interaction information. We found that hydrogen bonds, salt bridges, aromatic-aromatic interactions, and hydrophobic interactions are the main driving force of RhoA-GMP-PNP and Rh57 interaction, and the involved regions include Rh57's CDR3 and non-homologous complementary regions. The complex structure explained why Rh57 selectively binds to activated RhoA-GTP but not to inactivated RhoA-GDP and why Rh57's binding did not affect the downstream binding and activation of PRK1.

2. Materials and methods

2.1. Cloning and site-directed mutagenesis

The amino acid sequences of related proteins are listed in Table S1. The coding sequences of RhoA Q63L, Rh57, and Rh12 were optimized based on favored codon usage in *E. coli* and were synthesized by Generay (Generay Biotech Co., Ltd, Shanghai, China). For co-expression and crystallization, DNA encoding RhoA Q63L and Rh57 were subcloned into the pETDuet-1 vector, which is a co-expression vector. An N-terminal 8xHis tag followed by a SUMO tag was synthesized in front of RhoA Q63L, and a strep tag followed by a TEV protease cleavage site was synthesized in front of Rh57. DNA encoding Rh12 was subcloned into the same place as Rh57 by one-step PCR cloning. Besides, DNA encoding RhoA Q63L was subcloned into the pET28a-SUMO vector with an N-terminal 6xHis tag followed by a SUMO tag. DNA encoding Rh57 and Rh12 was subcloned into the vector with an N-terminal 8xHis tag followed by an MBP tag.

Site-directed mutagenesis of RhoA wt was carried out by employing PCR-based mutagenesis site-directed method (2x KOD One PCR Master Mix) (TOYOBO Inc., Japan) using pET28a-SUMO RhoA Q63L as the template. Site-directed mutagenesis of RhoA T19N was carried out by the same method using pET28a-SUMO RhoA wt as the template. The sequences of the primers used to obtain these mutants are displayed in Supplementary Table S2. The mutagenesis constructs were confirmed by DNA sequencing (GENEWIZ, Suzhou, China).

2.2. Protein expression and purification

For protein expression, the plasmids were transformed into *E. coli* strain BL21 (DE3). The bacteria were cultured in LB medium with 100 μg/ml ampicillin under 220 rpm shaking at 37 °C for 5 h. Recombinant protein expression was induced by 200 μM isopropyl-D-1-thiogalactopyranoside (IPTG) and incubation for an additional 20 h under 220 rpm shaking at 18 °C. The bacteria were harvested by centrifugation at 5000 rpm for 20 min, resuspended in NiA buffer containing 50 mM Tris-HCl, pH 8.0, 150 mM NaCl, 5% glycerol, and 20 mM imidazole. Especially, 0.5 mM GTP and 1 mM Mg^{2+} were added before the resuspending of cells expressing RhoA Q63L-Rh57 or RhoA Q63L-Rh12. Then the cells were lysed 5 times at 1000 bar and centrifugated at 18000 rpm at 4 °C. The supernatants containing His-tagged protein (RhoA Q63L-Rh57, RhoA Q63L-Rh12, RhoA Q63L, RhoA wt, and RhoA T19N) were purified by Ni-NTA affinity chromatography (Ni Sepharose 6 Fast Flow, GE Healthcare, UK), and the His-SUMO tag was removed by recombinant ULP1 overnight at 4 °C. The cleaved-tag protein effluent was concentrated by ultracentrifugation and finally purified by size-exclusion chromatography (SEC) (Superdex 200 Increase 10/300 GL, GE Healthcare, UK). Especially, 2 mM GMP-PNP (a non-hydrolyzable analog of GTP) was added to the concentrate containing RhoA Q63L-Rh57 or RhoA Q63L-Rh12 before size-exclusion chromatography. The supernatants containing MBP-tagged protein (MBP-Rh57 and MBP-Rh12) were purified by Amylose-resin affinity chromatography (Amylose resin, NEB, USA), eluted with buffer containing 50 mM Tris-HCl, pH 8.0, 150 mM NaCl, 5% glycerol, 20 mM imidazole, and 10 mM maltose, concentrated by ultracentrifugation and finally purified by size-exclusion chromatography (SEC) (Superdex 200 Increase 10/300 GL, GE Healthcare, UK). All the proteins were concentrated to 2–50 mg/ml in GF buffer containing 20 mM 4-(2-hydroxyethyl)-1-piperazineethanesulfonic acid (HEPES) pH 8.0 and 150 mM NaCl, flash-frozen in liquid nitrogen, and stored at −80 °C for further use. The molecular weight and purity of the target proteins were verified by SDS–PAGE.

2.3. Crystallization, data collection, determination, and refinement of RhoA-Rh57 complex structures

The protein sample used to obtain crystals contained 22 mg/ml RhoA Q63L-Rh57 and 1.2 mM GMP-PNP in GF buffer containing 20 mM HEPES pH 8.0 and 150 mM NaCl. RhoA Q63L-Rh57 complex crystals were obtained by vapor diffusion over a solution containing 20% (w/v) PEG 8000, 100 mM Tris base/Hydrochloric acid (pH 8.5), and 200 mM Magnesium chloride at 18 °C. Cryoprotection was performed by adding glycerol to the reservoir buffer at a 25% concentration. X-ray diffraction data were collected at beamlines BL02U1 [16], Shanghai Synchrotron Radiation Facility, Chinese Academy of Sciences.

The diffraction data were processed by XDS [17] and AIMLESS [18]. The structure of the RhoA Q63L-Rh57 complex was obtained by molecular replacement using PHENIX [19]. Protein Data Bank (PDB) ID code 1KMQ (for RhoA Q63L) [20] and 6ITQ (for nanobody) [21] were used as the search models. Refinement was performed with PHENIX [19], and adjustments were made with COOT [22]. The corresponding figures were drawn by PyMOL [23].

2.4. Nano differential scanning fluorimetry (NanoDSF)

For target proteins (RhoA wt, RhoA Q63L, RhoA T19N, MBP-Rh57, MBP-Rh12, RhoA Q63L-Rh57 complex, and RhoA Q63L-Rh12 complex), samples were prepared for 50 μl each in EP tubes and centrifuged at 12000 rpm at 4 °C for 10 min. The supernatants were transferred to new EP tubes. PR NT.48 capillaries were used to draw

Table 1
Data collection and refinement statistics. The values in parentheses are for the high-resolution shells.

Data collection	
PDB entry	7XQV
Space group	I 41 2 2
a, b, c (Å)	142.03, 142.03, 69.26
α, β, γ (°)	90, 90, 90
Resolution (Å)	50.22–2.76 (2.859–2.76)
Wilson B-factor	75.51
I/δ(I)	14.95 (1.21)
R_{merge}	0.4031 (4.569)
Completeness (%)	99.84 (100.00)
Number of unique reflections	9407 (924)
Reflections used for R-free	504 (53)
R_{work}	0.2187 (0.3483)
R_{free}	0.2648 (0.3982)
RMSD	
Bond length (Å)	0.002
Bond angle (°)	0.57
Average *B*, all atoms (Å^2)	78.07
Ramachandran plot	
Favored (%)	96.70
Allowed (%)	2.93
Outliers (%)	0.37
Rotamer outliers (%)	2.13

the samples from EP tubes to the nano differential scanning fluorimetry instrument (NanoDSF) (NanoTemper, Germany). For each sample, three groups of parallel experiments were carried out to reduce the error of the results. The parameters used in the experiment were 10% power and heating from 20 °C to 95 °C at a rate of 1 °C/min. The target protein's melting temperature (Tm) and aggregation temperature (Tagg) were determined with Prometheus PR Control software.

2.5. Verification of related proteins by dynamic light scattering (DLS)

Target protein samples (RhoA wt, RhoA Q63L, RhoA T19N, RhoA Q63L-Rh57 complex, and RhoA Q63L-Rh12 complex) were prepared for 50 μl each in EP tubes and centrifuged at 12000 rpm at 4 °C for 10 min. The cuvette was cleaned with 50 μl HEPES buffer 3 times. Ten μl HEPES buffer was added to the cuvette. The cuvette was placed into the instrument (DynaPro Nanostar) (Wyatt Technology, USA) to check whether the baseline was stable to determine the device's state. After confirming that the instrument was in good condition, a 10 μl sample was added to the cuvette and analyzed after the baseline was stable.

2.6. Verification of RhoA-Nb complexes by MALDI-TOF mass spectrometry

For mass spectrometry assay, a Superdex 200 Increase 10/300 GL column (GE Healthcare, UK) was used to exchange the buffer of RhoA Q63L-Nb complexes to 10 mM NH_4Ac. The molecular weight of protein samples was determined by linear mode matrix-assisted laser desorption/ionization-time of flight (MALDI-TOF) mass spectrometry.

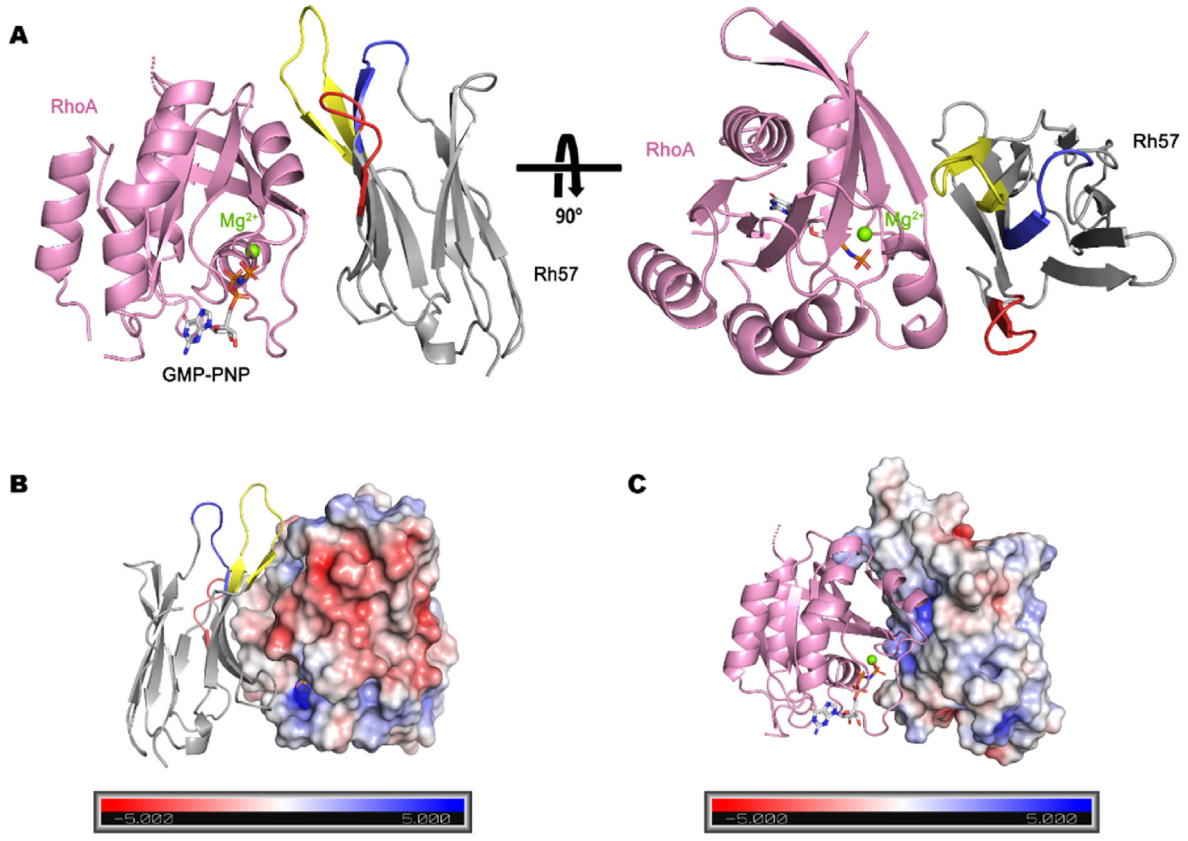

Fig. 1. Structure of GMP-PNP binding activated RhoA Q63L-Rh57 nanobody complex determined by X-ray crystallography. A. The overall structure of the RhoA-Rh57 complex. RhoA Q63L is shown in light pink. Rh57 is shown in light gray, and CDR1-3s are blue, red, and yellow. GMP-PNP is shown as stick-like structures. Mg^{2+} is shown in green. B&C. Electrostatic potential distribution at the molecular surface of RhoA-Rh57 complex (blue: positive, red: negative, white: neutral). B. Rh57 is shown in cartoon and C. RhoA is shown in cartoon. (For interpretation of the references to colour in this figure legend, the reader is referred to the Web version of this article.)

3. Results

3.1. The overall crystal structure of the RhoA-Rh57 complex

To gain insight information on how the nanobodies binding with GTP binding activated RhoA, recombinant RhoA, and RhoA-nanobody complex (RhoA Q63L-Rh57 complex, RhoA Q63L-Rh12 complex, RhoA Q63L, RhoA wt, and RhoA T19N) were purified by Ni-NTA affinity chromatography and size-exclusion chromatography (SEC) (Fig. S1 A-E & S2 A-G), the single symmetry SEC elution peak indicated that RhoA and the nanobodies formed a stable complex with 1:1 ratio. Further, the RhoA Q63L-Rh57 complex protein crystal was obtained through high-throughput screening (Fig. S3). Atomic-scale resolution crystal structure of GMP-PNP (an analog of GTP in which one of the oxygen atoms is replaced with an amine, thus cannot be hydrolyzed) binding activated RhoA with nanobody Rh57 was obtained using X-ray crystallography technology. We also crystallized the RhoA Q63L-Rh12 complex crystal. However, the crystal diffracted not well. The RhoA-Rh57 complex crystal contains RhoA Q63L, Rh57, and GMP-PNP at a 1:1:1 stoichiometry. The overall structure of RhoA-Rh57 has been refined to 2.76 Å resolution. The crystallographic data are shown in Table 1. The binding interface of CDR3 and non-hypervariable loop of Rh57 and RhoA was well defined. RhoA-Rh57 crystallized in the space group I 41 2 2, and the asymmetric unit contained one Rh57 nanobody, one RhoA molecule, one GMP-PNP molecule, and one Mg^{2+}. The structure was deposited to PDB with ID: 7XQV.

Fig. 1A shows the overall structure of the RhoA-Rh57 complex, which captured the nanobody Rh57 interacting with GMP-PNP binding activated RhoA. Fig. 1B and C shows the electrostatic potential distribution on the surface of RhoA and Rh57, respectively. Rh57 nanobody side chain is positively charged near the contact surface, while the RhoA binding surface is negatively charged, indicating that electrostatic interactions also contribute to forming a highly stable complex.

3.2. Details of the binding sites of Rh57 to RhoA

The binding surface between RhoA Q63L and Rh57 is shown in Fig. 2. In the RhoA-Rh57 complex, CDR3 and the non-hypervariable loop of Rh57 contributed to the binding to RhoA Q63L. Most of the interactions are attributed to hydrogen bonds, salt bridges, aromatic-aromatic interactions and hydrophobic interactions formed at the binding interface. In Rh57 CDR3 (Fig. 2B), salt bridges were formed between Arg109 and RhoA's Asp78. Besides, hydrogen bonds were formed between Rh57's Thr110 and RhoA's Asp76 (2.88 Å) and Lys7 (3.53 Å). In the non-hypervariable loop (Fig. 2C), hydrogen bonds were formed between Arg48 and RhoA's Glu40 and Asn41. Salt bridges were also formed between Rh57's Glu47 and RhoA's Lys27, Rh57's Arg48 and RhoA's Glu40. A hydrophobic aromatic pocket is formed by the side chain of Rh57's Phe40, Phe50, Ala53 (CDR2), Ile102 (CDR3), and Trp112 (CDR3). This hydrophobic pocket interacts with and recognizes the side chain of RhoA's Phe39, which belongs to the SWI region. Rh57's Glu47 has a hydrogen bond with RhoA's Gln29, and Phe50 also has hydrophobic interaction with RhoA SWI's Val38.

Although Rh57's CDR1 did not directly contribute to the binding of Rh57 to RhoA, Trp32 in CDR1 formed aromatic-aromatic interaction with Trp101 and Tyr113 of CDR3, thus helping the CDR3 maintain a specific conformation. The total calculated buried surface areas of Rh57 to RhoA is 837.4 $Å^2$ by PISA, larger than several other nanobodies (e.g., LaM2-mCherry 679.6 $Å^2$ in 6IR2, LaM4-mCherry, 757.8 $Å^2$ in 6IR1, LaG16-GFPuv 700.0 $Å^2$ in 6LR7, and Nb2-sfGFP 648.8 $Å^2$ in 7E53), showing the interaction between Rh57 and RhoA is somehow strong among the typical nanobodies [24–27].

We also investigated the interaction between RhoA and GMP-PNP after Rh57's binding. The binding of Rh57 did not significantly interfere with the interaction between RhoA and GMP-PNP. RhoA's Cys16, Gly17, Lys18, Thr19, Cys20, Tyr34, Thr37, Gly62, Lys118, Asp120, Ser160, Ala161, and Lys162 contribute to the interaction with GMP-PNP. The total buried surface of the binding is 439.3 $Å^2$, calculated by PISA.

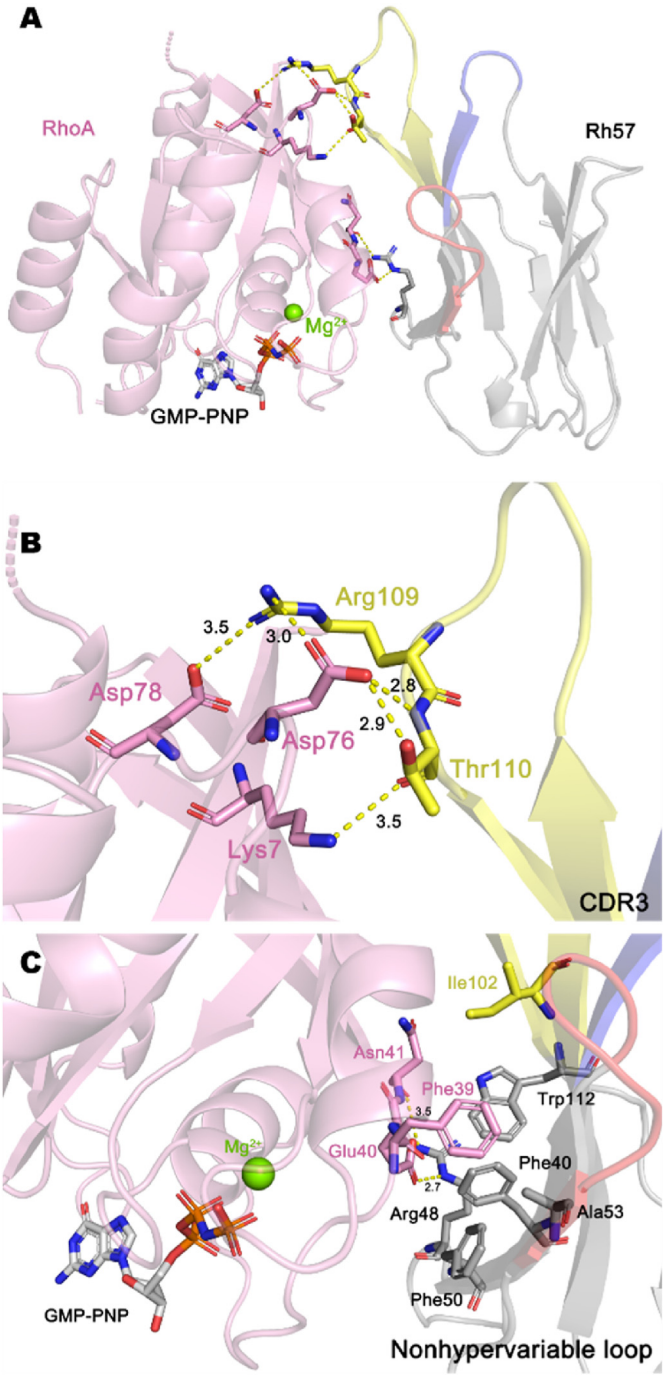

Fig. 2. The detailed binding interfaces of Rh57 to RhoA Q63L. (A) View of the overall binding interface between Rh57 and RhoA. (B–C) View of Rh57's CDR3-RhoA and non-hypervariable loop-RhoA interaction interfaces. Residues of the interaction interface are represented as stick-like structures. The yellow dashed lines indicate the major interaction areas between Rh57 and RhoA. (For interpretation of the references to colour in this figure legend, the reader is referred to the Web version of this article.)

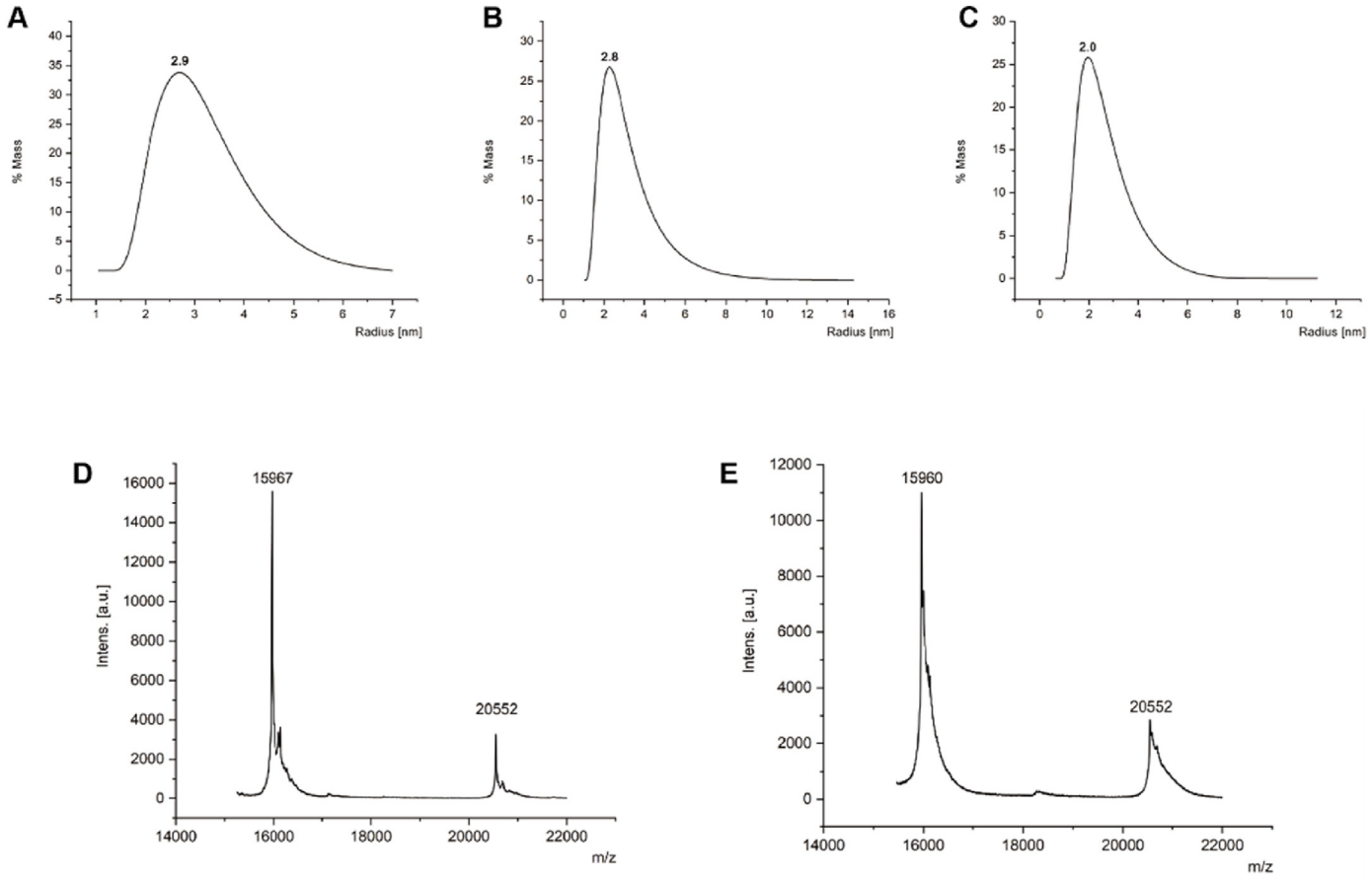

Fig. 3. Verify the formation of the RhoA-nanobody complex. The dynamic light scattering results of (A) RhoA Q63L-Rh57 complex solution; (B) RhoA Q63L-Rh12 complex solution; (C) RhoA Q63L solution without nanobody; The MALDI-TOF mass spectrometry result of (D) RhoA Q63L-Rh57 complex and (E) RhoA Q63L-Rh12 complex. The first m/z peak shows Rh57 or Rh12, and the second peak shows the RhoA Q63L.

3.3. Thermal stability of related proteins measured by NanoDSF

We compared the stability of RhoAs, Nbs, and RhoA-Nbs by NanoDSF (nano differential scanning fluorimetry). NanoDSF can determine protein stability by employing intrinsic tryptophan or tyrosine fluorescence with minimal samples [28]. Fig. S4 and Table S3 show the Tm (midpoint temperature of thermal unfolding) and Tagg (onset temperature of aggregation) values of the target proteins. The average Tm values for RhoA wt, RhoA Q63L, RhoA T19N, MBP-Rh57, MBP-Rh12, RhoA Q63L-Rh57, and RhoA Q63L-Rh12 are 56.8 °C, 68.1 °C, 43.8 °C, 54.1 °C, 53.8 °C, 46.3 °C, and 68.4 °C, respectively. Among the RhoAs investigated, RhoA Q63L exhibited the highest Tm, which means it was the most stable RhoA variant. MBP-Rh57 and MBP-Rh12 had similar Tm. As for the complex, the RhoA Q63L-Rh12 complex exhibited a higher Tm than monomer protein, which means it was more stable. However, the RhoA Q63L-Rh57 complex showed a lower Tm than monomer protein. It also had two inflection points for ratio, which suggests that the conformational change of the complex is more complex during denaturation, and there may be some intermediates state.

3.4. Verify the RhoA-nanobody complex by dynamic light scattering (DLS) and MALDI-TOF mass spectrometry

The binding ratio of Rh57 to activated RhoA and if it will form larger oligomers were also verified by dynamic light scattering. Samples of RhoA Q63L, RhoA-Rh57, and RhoA-Rh12 protein solutions at a 1 mg/ml concentration were measured. Fig. 3A-C and Table S4 show the detailed information. The measured molecular weights of particles in RhoA Q63L, RhoA-Rh57, and RhoA-Rh12 solutions are 23.8 kD, 41.3 kD, and 35.9 kD, and their theoretical molecular weights are 20.6 kD, 36.5 kD, and 36.5 kD, respectively. Considering that molecular weight data were calculated from the measured particle radius, it can be regarded that the measured results are consistent with the theoretical size. Pd (%) shows that the reliability of the obtained data is relatively reliable. Mass (%) shows the percentage of the particles at the peak in all the tested particles in the solution. The Mass (%) values of all groups are above 99%, showing that all the testes RhoA Q63L, RhoA-Rh57, and RhoA-Rh12 exist as monomers in the solution are those we expected. DLS results demonstrated that the binding between RhoA and nanobodies is relatively stable. The complex proteins are stable and did to tend to form oligomers or aggregates, which is essential to prevent false-positive results caused by the nanobody's aggregation. The RhoA-Rh57 and RhoA-Rh12 complexes were further verified by MALDI-TOF mass spectrometry (Fig. 3D & E). However, in the harsh mass spectrometry testing condition, the RhoA-nanobody complex dissociated, and the single protein m/z peaks in accord with the calculated theoretical molecular weight.

4. Discussion

Due to the importance of RhoA in cells and its relationship with cancer pathogenesis, the research on RhoA is of great significance.

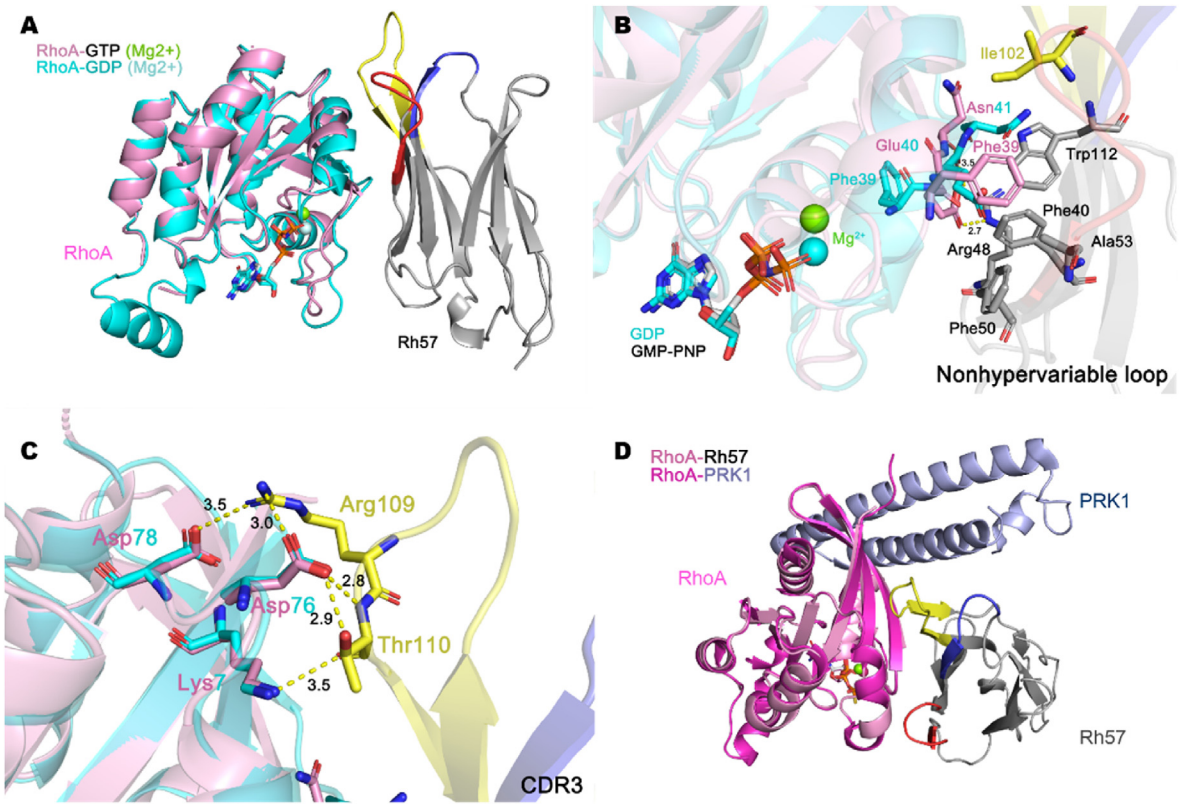

Fig. 4. Rh57 selectively binding to RhoA-GTP and does not affect RhoA binding to the PRK1 effector domain. (A–C) The alignment of GTP-bound active RhoA-Rh57 with GDP-bound inactivated RhoA. RhoA in the GTP-bound state is light pink and cyan in the GDP-bound form. The two structures are superimposed to compare the detailed binding interface. The residues involved in the interaction interface are shown as sticks. The yellow dashed line indicates the interactions including hydrogen bonds and salt bridges. (D) The alignment of the RhoA-Rh57 complex structure with the RhoA-PRK1 effector domain complex. RhoA Q63L of RhoA-Rh57 is shown in light pink, Rh57 is shown in gray, its CDR1-3s are shown in blue, red, and yellow, and Mg^{2+} is shown in green, GMP-PNP is shown as stick-like structures. RhoA G14V of RhoA-PRK1 is shown in cyan, PRK1 effector domain is shown in light purple, Mg^{2+} is shown in green, and GTPγS is shown as stick-like structures. (For interpretation of the references to colour in this figure legend, the reader is referred to the Web version of this article.)

Considering that the defects of existing molecular tools limit the inhibitor screening of RhoA, and nanobodies have many advantages as a research hotspot of artificial antibodies in recent years, the research on RhoA-specific nanobodies is of great significance. Previously, Olichon and colleagues screened out Rh57, which binds to RhoA without affecting its function [9]. Our work determined the structure of the RhoA-Rh57 complex and the detailed binding information of how Rh57 interacts with activated GTP binding RhoA. RhoA and Rh57 interact mainly through hydrogen bonds, salt bridges, aromatic-aromatic interactions, and hydrophobic interactions. We found that the CDR3 and the nonhypervariable region of Rh57 bind to the SWI and SWII switch loops of RhoA, respectively. When RhoA binds to GDP [26] or GTP, the two switch loops undergo a conformational change. We compared the structure of active RhoA-Rh57 with inactive GDP bound RhoA PDB ID: 1FTN (Fig. 4A–C). RhoA's Phe39 sidechain points to different directions between GDP and GTP bound form. The GDP's binding will move the RhoA's Phe39 out of Rh57's hydrophobic aromatic pocket. RhoA binds to GDP will disrupt the hydrophobic interaction between RhoA SWI switch's Val38 and Rh57's Phe50. Also, the GDP's binding will disrupt the hydrogen bond between GTP-bound RhoA's Gln29 and Rh57's Glu47, as well as the hydrogen bonds and salt bridges formed by Rh57's Arg48 and RhoA's Glu40 and Asn41. Therefore, Rh57 can selectively recognize these changes and interact with GTP binding activated RhoA but not with the GDP binding inactivated RhoA.

We are also interested in the mechanism of why the binding of Rh57 did not interfere with the downstream signaling pathway. Although the trial of co-crystallization of another RhoA-Rh12 complex that will affect the downstream signaling pathway did not get a good crystal suitable for diffraction, we can still get plenty of clues from the RhoA-Rh57 complex. We compared the structure of the RhoA-Rh57 complex with the structure of the RhoA-PRK1 effector domain complex (PDB ID: 1CXZ [29]) (Fig. 4D). PRK1 (PKN) is a downstream serine/threonine protein kinase that is controlled by activated RhoA [30], and previous studies have shown that PRK1 plays a vital role in the assembly or stabilization of cytoskeletal proteins [31]. We found no direct contact between Rh57 and PRK1 effector domains, and the epitopes that Rh57 recognized with RhoA do not overlap with PRK1, which may prove that Rh57 does not interfere with the binding of RhoA and PRK1 effector domains. It may also be the reason why Rh57 does not affect the activity of RhoA in cells: the binding of Rh57 nanobody did not interfere with the further binding of the downstream effectors of RhoA.

In addition, we analyzed the thermal stability and solution particle information of related proteins using NanoDSF, DLS, and MALDI-TOF mass spectrometry. These results showed that the RhoA and Rh57 form a stable complex, and the molar ratio is 1:1. Rh57 is indeed a promising candidate for the RhoA intracellular biosensor. However, Rh57 itself is easy to form oligomers and aggregates. The structural analysis showed this might be related to the interaction between Trp107, Tyr57, and Ser78, which may form hydrogen bonds/ aromatic-aromatic interactions/ hydrophobic

interactions and cause self-aggregate. Rh57's CDR2 only had hydrophobic interaction with RhoA; while they are very close, further mutation of this region may provide additional specific interaction and improve the binding affinity of the nanobody. Thus, Rh57 may be further engineered to a better nanobody with higher binding affinity and selectively binding with activated RhoA.

Author contributions

YD conceived and supervised the study; YZ, ZW, PZ, and RL performed protein purification, verification, crystallization, and crystal data analysis; SC performed protein purification and validation; YZ wrote the draft manuscript; YD and RL made manuscript revisions.

Declaration of competing interest

We declare that we have no conflicts of interest in the authorship or publication of this contribution.

Acknowledgments

This work was supported by grants from the National Natural Science Foundation of China (32070939 and 82030106), the Innovative Research Team of High-Level Local Universities in Shanghai, and the Key Laboratory Program of the Education Commission of Shanghai Municipality (ZDSYS14005).

Appendix A. Supplementary data

Supplementary data to this article can be found online at https://doi.org/10.1016/j.bbrc.2022.05.084.

References

[1] K. Wennerberg, K.L. Rossman, C.J. Der, The Ras superfamily at a glance, J. Cell Sci. 118 (5) (2005) 843–846.
[2] R.G. Hodge, A.J. Ridley, Regulating Rho GTPases and their regulators, Nat. Rev. Mol. Cell Biol. 17 (8) (2016) 496–510.
[3] S. Etienne-Manneville, A. Hall, Rho GTPases in cell biology, Nature 420 (6916) (2002) 629–635.
[4] A.J. Ridley, Rho family proteins: coordinating cell responses, Trends Cell Biol. 11 (12) (2001) 471–477.
[5] E. Sahai, C.J. Marshall, RHO-GTPases and cancer, Nat. Rev. Cancer 2 (2) (2002) 133–142.
[6] F.M. Vega, A.J. Ridley, Rho GTPases in cancer cell biology, FEBS (Fed. Eur. Biochem. Soc.) Lett. 582 (14) (2008) 2093–2101.
[7] A.L. Bishop, A. Hall, Rho GTPases and their effector proteins, Biochem. J. 348 (2) (2000) 241–255.
[8] X. Shang, et al., Rational design of small molecule inhibitors targeting RhoA subfamily Rho GTPases, Chem. Biol. 19 (6) (2012) 699–710.
[9] L. Keller, et al., Selection and characterization of a nanobody biosensor of GTP-bound RHO activities, Antibodies 8 (1) (2019) 8.
[10] C. Hamers-Casterman, et al., Naturally occurring antibodies devoid of light chains, Nature 363 (6428) (1993) 446–448.
[11] P.C. Fridy, et al., A robust pipeline for rapid production of versatile nanobody repertoires, Nat. Methods 11 (12) (2014) 1253–1260.
[12] S. Muyldermans, Nanobodies: natural single-domain antibodies, Annu. Rev. Biochem. 82 (1) (2013) 775–797.
[13] C. Leow, et al., Single domain antibodies as new biomarker detectors, Diagnostics 7 (4) (2017) 52.
[14] F. Peyvandi, et al., Caplacizumab for acquired thrombotic thrombocytopenic purpura, N. Engl. J. Med. 374 (6) (2016) 511–522.
[15] S. Moutel, et al., NaLi-H1: a universal synthetic library of humanized nanobodies providing highly functional antibodies and intrabodies, Elife 5 (2016) e16228.
[16] Q.S. Wang, et al., Upgrade of macromolecular crystallography beamline BL17U1at SSRF, Nucl. Sci. Tech. 29 (5) (2018) 7.
[17] W. Kabsch, Xds, Acta Crystallogr. D: Biol. Crystallogr. 66 (2) (2010) 125–132.
[18] M.D. Winn, et al., Overview of the CCP4 suite and current developments, Acta Crystallogr. Sect. D Biol. Crystallogr. 67 (4) (2011) 235–242.
[19] P.D. Adams, et al., PHENIX: a comprehensive Python-based system for macromolecular structure solution, in: Acta Crystallographica Section D-Biological Crystallography, 2012, pp. 539–547.
[20] K. Longenecker, et al., Structure of a constitutively activated RhoA mutant (Q63L) at 1.55 Å resolution, Acta Crystallogr. Sect. D Biol. Crystallogr. 59 (5) (2003) 876–880.
[21] L. Ding, et al., Structural insights into the mechanism of single domain VHH antibody binding to cortisol, FEBS (Fed. Eur. Biochem. Soc.) Lett. 593 (11) (2019) 1248–1256.
[22] P. Emsley, et al., Features and development of coot, Acta Crystallogr. Sect. D Biol. Crystallogr. 66 (4) (2010) 486–501.
[23] W.L. DeLano, J.W. Lam, PyMOL: A Communications Tool for Computational Models, 1155 16TH, AMER CHEMICAL SOC, ST, NW, WASHINGTON, DC 20036 USA, 2005.
[24] E. Krissinel, K. Henrick, Inference of macromolecular assemblies from crystalline state, J. Mol. Biol. 372 (3) (2007) 774–797.
[25] Z. Wang, et al., Structural insights into the binding of nanobodies LaM2 and LaM4 to the red fluorescent protein mCherry, Protein Sci. 30 (11) (2021) 2298–2309.
[26] Z. Zhang, et al., Structure-based engineering of anti-GFP nanobody tandems as ultra-high-affinity reagents for purification, Sci. Rep. 10 (1) (2020) 1–10.
[27] P. Zhong, et al., Structural insights into two distinct nanobodies recognizing the same epitope of green fluorescent protein, Biochem. Biophys. Res. Commun. 565 (2021) 57–63.
[28] P. Linke, et al., An automated microscale thermophoresis screening approach for fragment-based lead discovery, J. Biomol. Screen 21 (4) (2016) 414–421.
[29] R. Maesaki, et al., The structural basis of Rho effector recognition revealed by the crystal structure of human RhoA complexed with the effector domain of PKN/PRK1, Mol. Cell 4 (5) (1999) 793–803.
[30] P. Flynn, et al., Multiple interactions of PRK1 with RhoA. Functional assignment of the Hr1 repeat motif, J. Biol. Chem. 273 (5) (1998) 2698–2705.
[31] T. Kawamata, et al., A protein kinase, PKN, accumulates in alzheimer neurofibrillary tangles and associated endoplasmic reticulum-derived vesicles and phosphorylates tau protein, J. Neurosci. 18 (18) (1998) 7402–7410.